

## **FULL-SCALE TESTING OF FUSELAGE PANELS**

Dr. John G. Bakuckas, Jr., FAA-TC, (609) 485-4784, [john.bakuckas@faa.gov](mailto:john.bakuckas@faa.gov)

Dr. Catherine A. Bigelow, FAA-TC, (609) 485-6662, [cathy.bigelow@faa.gov](mailto:cathy.bigelow@faa.gov)

Dr. Paul W. Tan, FAA-TC, (609) 485-6662, [paul.tan@faa.gov](mailto:paul.tan@faa.gov)

Prof. Jonathan Awerbuch, Drexel University, (215) 895-2291, [awerbuch@coe.drexel.edu](mailto:awerbuch@coe.drexel.edu)

Prof. Alan C. Lau, Drexel University, (215) 895-2377, [lau@drexel.edu](mailto:lau@drexel.edu)

Prof. T. M. Tan, Drexel University, (215) 895-2293, [tan@drexel.edu](mailto:tan@drexel.edu)

### **ABSTRACT**

A unique state-of-the-art facility to assess the structural integrity of aircraft fuselage structure was established at the Federal Aviation Administration (FAA) William J. Hughes Technical Center. The Full-Scale Aircraft Structural Test Evaluation and Research (FASTER) facility is capable of testing full-scale fuselage panel specimens under conditions representative of those seen by an aircraft in actual operation. The test fixture features a novel adaptation of mechanical, fluid, and electronic components and is capable of applying pressurization, longitudinal, hoop, frame, and shear loads to a fuselage panel. A high-precision, Remote Controlled Crack Monitoring (RCCM) system was developed to inspect and record crack initiation and progression over the entire fuselage panel test surface. A detailed description of the FASTER facility along with representative results from a variety of experimental test programs will be presented.

Keywords: Multiple-site cracks, strain survey, fatigue crack growth, residual strength, crack bulging.

### **1 INTRODUCTION**

The development of experimental and analytical methodologies to assess multiple-site cracking scenarios and other phenomena associated with aging aircraft structure has been the focus of numerous research activities in the aircraft industry over the past decade. Many of these efforts were precipitated by the 1988 Aloha Airlines Accident in which a large portion of the fuselage crown of a Boeing 737 tore apart due to the occurrence and sudden link-up of small cracks emanating from rivet holes in the lap joint. The Federal Aviation Administration (FAA), National Aeronautics and Space Administration (NASA) and Department of Defense (DoD) have sponsored research efforts addressing this complex problem on several fronts. This includes the development of various analytical tools, complex numerical methods, and simplified engineering approaches to predict crack initiation, crack growth and link-up, and residual strength [1-9]. Each tool is capable of analyzing portions of the multiple-site crack initiation, growth, link-up, and catastrophic fracture process in fuselage structure. Combined, these tools

can predict the entire process and can be used for future aircraft designs to prevent the occurrence of multiple-site cracking within the design life goal.

Computational tools must be verified and validated using experimental data to ensure successful transfer of useable and accurate technology to industry. The Full-Scale Aircraft Structural Test Evaluation and Research (FASTER) facility, located and operated at the FAA William J. Hughes Technical Center, was established to provide experimental data to support and validate analytical methods under development, including widespread fatigue damage (WFD) prediction, repair analysis and design, and new aircraft design methodologies. The system was designed using commercial-off-the-shelf (COTS) components whenever possible and to operate in an environment requiring minimal infrastructure support. The system was designed with safety considerations in mind by using water as the loading media. Using a simple loading mechanism consisting of levers, fulcrums, and water actuators, complex mechanical loading is economically introduced. This simplified mechanical design concept, in conjunction with a computer control and data acquisition system, presents a test system that is user friendly, has low-cost maintenance, is inherently safe, and is highly versatile.

The FASTER test fixture is capable of applying realistic flight load conditions to large sections of a fuselage structure. Both quasi-static and long-term durability spectrum loadings can be applied, including differential pressure, longitudinal, hoop, and shear load in the skin, and hoop load in the frames. This paper reports the novel features of the FASTER facility and test and analyses results obtained for typical narrow-body fuselage structure consisting of skin, frames, shear clips, stringers, and either longitudinal splice or circumferential joints. Strain survey tests were conducted under quasi-static loading conditions on test panels to verify proper load transfer from the load application points to the panel. Comparison with an independent full-scale test conducted on an aft fuselage section of an actual aircraft with similar structural details to the panels tested in this program and comparisons with detailed finite element analysis confirmed appropriate applied load conditions. Crack growth under fatigue loading conditions was measured and recorded using the Remote Control Crack Monitoring (RCCM) system up to a predetermined crack length. Finally, crack extension and residual strength were measured under quasi-static loading conditions. In the following sections, a brief description of the FASTER test fixture is presented followed by the analytical and experimental results including strain distributions, damage growth process, and residual strength characteristics.

## **2 DESCRIPTION OF FACILITY**

The FASTER test fixture, shown in Figure 1, features a unique adaptation of mechanical, fluid, and electronic components and is capable of applying internal pressurization, longitudinal, hoop, frame, and shear loads to a curved panel. As shown in the exploded view in Figure 2, the fixture consists of a base structure, hoop load assembly, longitudinal load assembly, fuselage pressure box, frame load assembly, and shear fixture assembly. The FASTER facility also includes a computerized instrument control and data acquisition system and a remote-controlled video system. A complete description is provided in reference 10, and an overview is introduced here in.

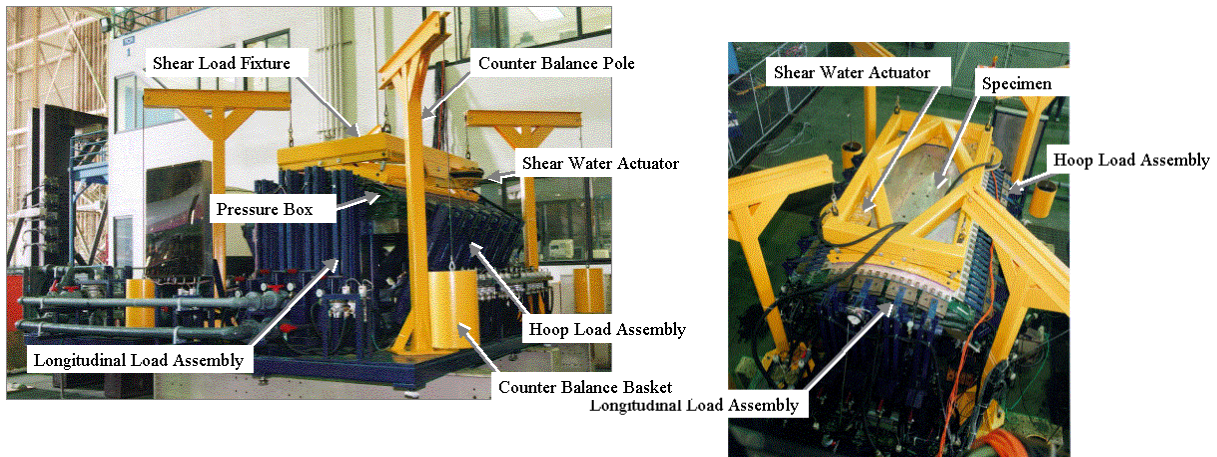


**Figure 1.** Photographs of FASTER fixture

In general, the test fixture is capable of dynamically cycling the internal pressure as well as performing a static pressurization. The hoop and longitudinal stresses are simulated by the controlled application of distributed loads around the perimeter of the test panel. Hoop forces are distributed by individual loading linkages using a two-tier coaxial whiffle tree assembly, which generates four equal forces from each controlled load point. A total of seven load points are used on each side of the specimen, creating a total of 28 attachment points. Longitudinal forces are applied using similar loading devices on each end of the panel, consisting of four load control points and 16 attachment points. Similar devices are available to apply hoop tension loads at each end of a frame.

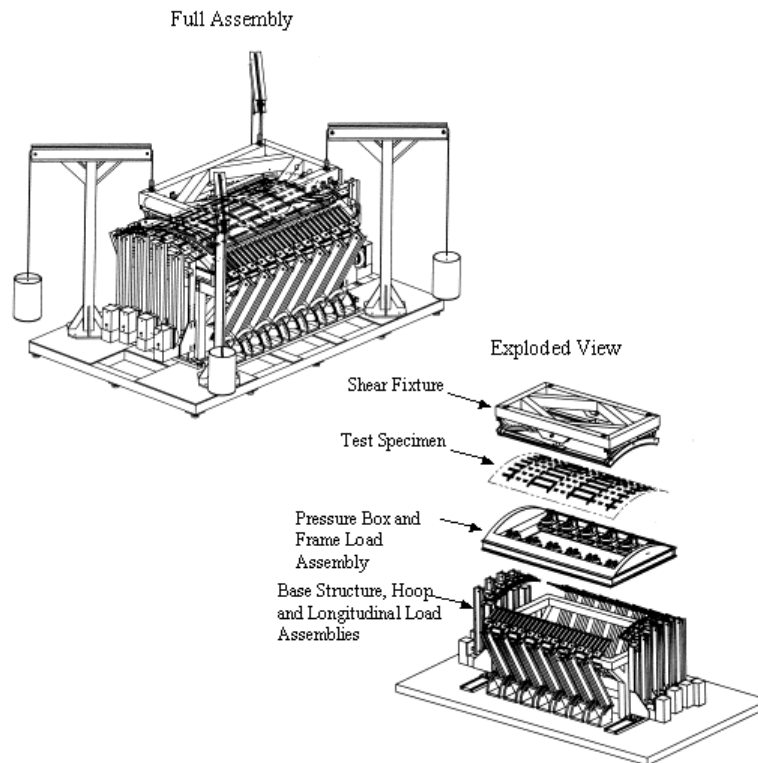


**Figure 2.** Full-Scale Aircraft Structural Test Evaluation and Research fixture

An innovative shear load application system was developed that uses two load distribution points in the longitudinal direction at the edges of the specimen. The force is applied as a couple and is reacted by a couple in the hoop direction. A unique feature of the shear loading system is the elastomeric coupling between the loading mechanisms and the test specimen. The elastomer, which has a soft shear modulus, creates a close approximation to uniform shear distribution in both the applied and reacted couples.

All forces are generated using water and air as the fluid medium. The external loads are generated by applying water pressure to bladder type actuators, which are controlled by pressure-activated dome valves. The dome valves are automatically controlled by electro/pneumatic (E/P) control valves. The E/P valves are driven by a computer control system in a closed-loop configuration. The operator can control the loads, speed, and type of test. Data from strain gages, load transducers, pressure transducers, etc., are displayed on color monitors in real time, and stored for off-line analysis.

## 2.1 Mechanical Loading Mechanisms

Water actuators, with a lever-arm construction, are used to apply loads to the curved panel. The water actuators used are air-water springs. An air-water spring is an elastomeric rubber fabric bellows with metal-end closures which contains a column of compressed air or water. In the FASTER test fixture, water is used. The compressed water provides the force or supports the load. Air-water springs have wide industrial applications including vibration isolation, truck suspension, and actuators. They are highly durable, rugged, and reliable. The water actuators used for the FASTER test fixture are more cost-effective than the standard oil-based hydraulic cylinder actuators. The initial purchase cost is much less and no maintenance or lubrication is required. There is no internal rod or piston or sliding seals, as in conventional cylinders. Since there are no moving parts in the water actuator, it is friction free and response is immediate.

A schematic of the general loading mechanism for the longitudinal and hoop load assemblies is shown in Figure 3. The loading mechanism consists of a water actuator, lever arm, fulcrum

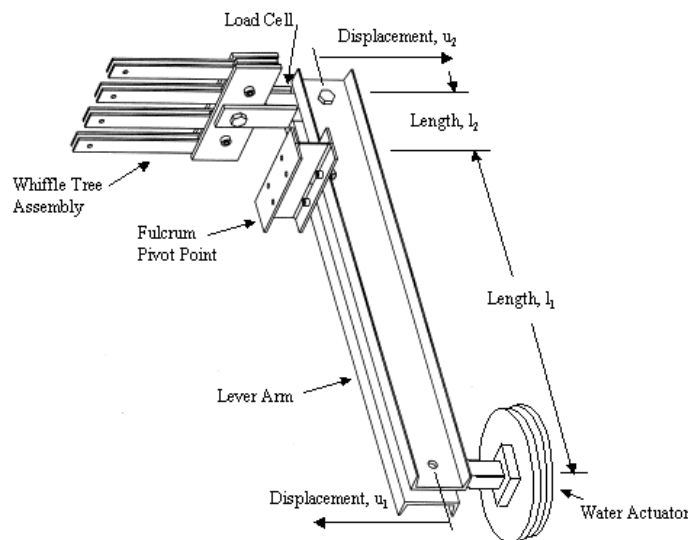


**Figure 3.** Schematic of longitudinal and hoop loading mechanism

pivot point, a load cell, and a whiffle tree. The lever arm is connected to the water actuator at one end and to the load cell at the other and rotates about the fulcrum pivot point. The distance from the water actuator to the fulcrum is  $l_1$ , and the distance from the top of the lever arm to the fulcrum is  $l_2$ . As the water actuator inflates, the bottom of the lever arm will displace an amount  $u_1$ , rotate at the fulcrum pivot point, causing the top of the lever arm to displace an amount  $u_2$ . There are eight loading mechanisms to apply longitudinal load, four attached to each end of the specimen, as shown in Figure 2. There are fourteen loading mechanisms to apply the hoop load, seven on each side of the specimen. The load is distributed to the edge of the specimen through four links in the whiffle tree for each loading mechanisms, as shown in Figure 3.

The shear load assembly consists of the shear fixture and four counterbalance poles and baskets, as shown in Figure 4. The shear fixture consists of a rigid reaction structure and pairs of water actuators, shear lever arms, pivot points, longitudinal skis, and hoop skis. The longitudinal and hoop skis are attached to the curved panel using an elastic 1"-thick by 4"-wide polyurethane

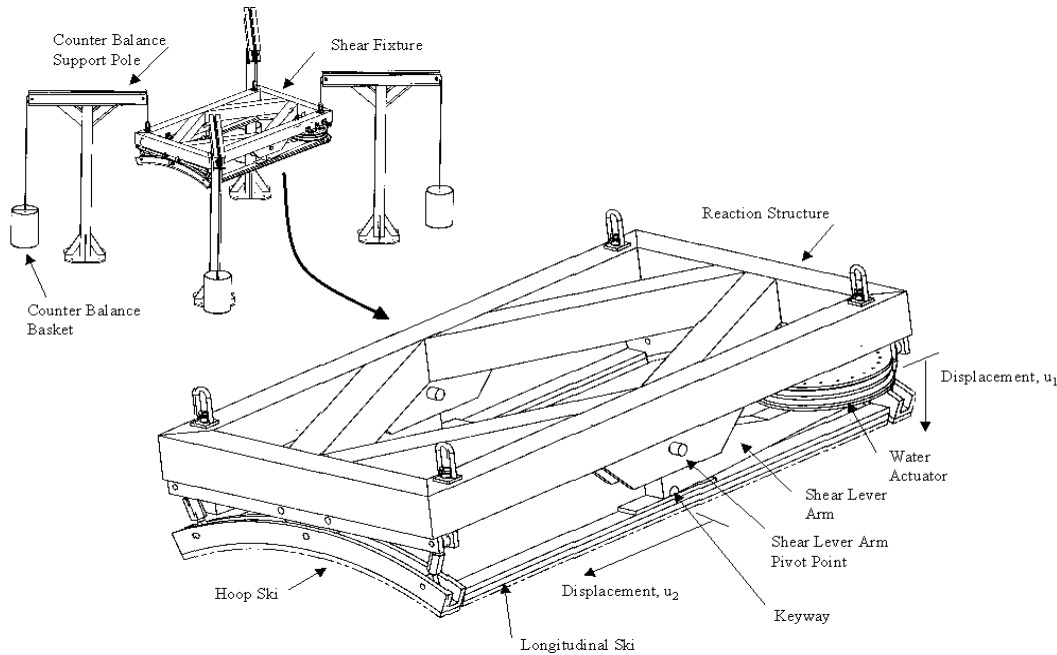


**Figure 4.** Schematic of shear loading mechanism

strips with a Shore A durometer scale hardness rating of 90. These strips are a hard rubber material on the Shore A scale compared to rubber bands at 40, tire treads at 50, and shoe heels at 70. As the water actuator inflates, the shear lever arm will displace downward,  $u_1$ , and will rotate about the shear arm pivot point. As a result, the lever arm keyway, which is attached to longitudinal ski, will displace amount  $u_2$  as shown in Figure 4. The displacement  $u_2$ , will deform the polyurethane strip that will distribute the point force at the keyway into a uniform shear force distributed along the entire length of the longitudinal ski. By inflating the two water actuators, which are located at diagonal corners of the reaction structure, the shear loads are applied through the longitudinal skis in equal magnitude but opposite direction. The shear couple is reacted by the rigid support structure, which is attached to the hoop skis. The entire shear load fixture weighs approximately 3800 lbs. To insure this weight is not applied to the panel, the

fixture is counter balanced using four weights attached to the fixture through four cable support columns, as shown in Figure 4.

The frame load assembly loading mechanism is shown in Figure 5. The figure shows a cut-away view through a frame loader. The frame loading mechanism consists of a water actuator, a frame lever arm, a fulcrum pivot point, a radial reaction link and a frame load link. As the water actuator inflates, the end of the frame lever arm will displace an amount  $u_1$  and will cause a displacement of the frame load link in the hoop direction,  $u_2$ . The radial reaction link ensures that the frame attachment point is displaced only in the hoop direction. There are 12 loading mechanisms for the frame load assembly.

The curved panel can be pressurized using either air, water, or a combination of both. The panel skin is attached to the pressure box using an elastomeric rubber seal, as shown in Figure 5. The seal is bonded to the panel skin and bolted to the pressure box.

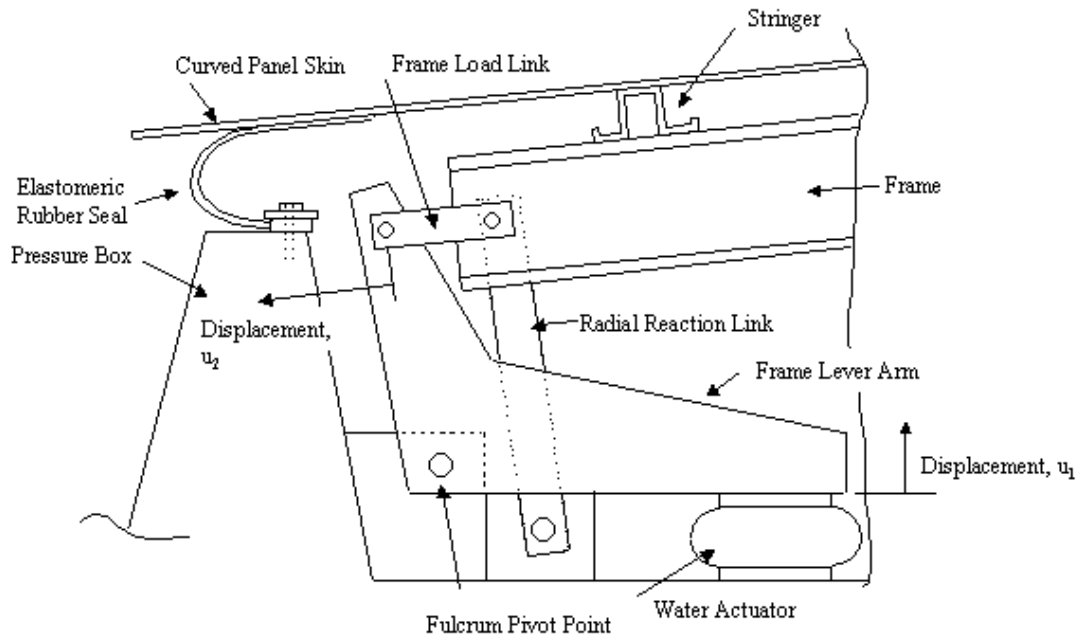


**Figure 5.** Schematic of frame loading mechanism

## 2.2 Hydraulic and Pneumatic Systems

All forces are generated using water supplied by a stand-alone water system. The water supply system consists of a 1050-gallon reservoir and a 40-horsepower pump capable of discharging water at 140-psi pressure. A radiator on the water return line acts as a heat exchanger to keep the water temperature below 105°F. Under normal operating conditions, 60 psi is a sufficient operational pressure.

A schematic of the hydraulic and pneumatic system for a single loading mechanism is shown in Figure 6. The pressure regulator dome valves use the air pressure applied above the valve diaphragm controlled by the E/P valves to accurately regulate water outlet pressure used to inflate the water actuator. When the water actuator deflates, the water exits to the water return

manifold through a constant flow orifice valve. The water outlet pressure is identical to the air inlet pressure applied to the dome above the diaphragm. The E/P valves convert a 0- to 10-volt control input signal to a proportional 0.7- to 127 psi pneumatic air pressure inlet signal sent to the pressure regulator dome valves. An air compressor supplies air to the E/P valves at a pressure of 130 psi. The E/P valves are computer controlled as discussed in the next section.

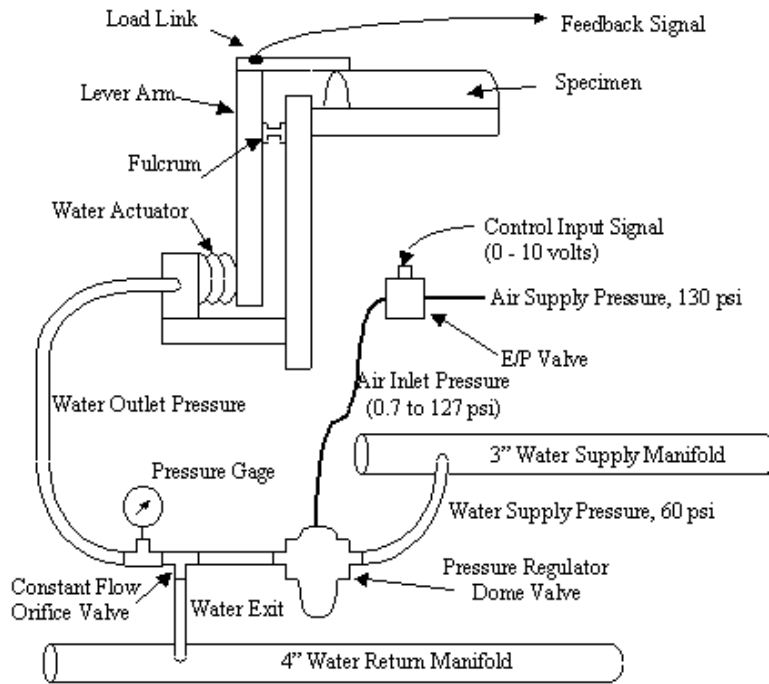


**Figure 6.** Schematic of the hydraulic and pneumatic system

### 2.3 Control and Data Acquisition Instrumentation

The computer control and data acquisition instrumentation integrates the various mechanical load assemblies of the FASTER test fixture. The control and data acquisition instrumentation uses the VXIbus (VMEbus eXtensions for Instrumentation) standard. The VXIbus standard provides the architecture for low-level analog signals to coexist on the backplane with high-speed digital signals resulting in state-of-the-art test and measurement instrumentation with high throughput and versatility.

The control and data acquisition instrumentation contains a six-slot VXI mainframe (HP1421B). In the current configuration, five slots are used for control and data acquisition with one reserved for expansion. The zero slot contains a UNIX-based VXI embedded controller (HP V732/100) with a 100-MHz RISC processor. The next four slots of the mainframe contain VXI multifunction measurement and control (HP E1419A) modules having 16-bit measurement resolution and 56,000 samples per second maximum reading rate. The HP E1419A module can be configured for a specific measurement and control application by using up to eight signal conditioning plug-on (SCP) cards. The SCP cards can accommodate up to eight input or output channels and can provide various analog and digital input or output functions. In the first slot, the E1419A module is designed for control of the longitudinal load assemblies, internal panel

pressure, the shear load assemblies, and system hydraulic supply. In the second and third slots, the E1419A modules have similar configurations, each designed for the control of the hoop and frame load assemblies on both sides of the system. In the fourth slot, the E1419A is designed for 64 channels of data acquisition with 56 low-level signals with a gain of 64 used for strain and crack propagation gages and eight high-level signals for pressure transducers.

The scanning rate of the control and data acquisition process is 150 times per second. There are 64 channels dedicated to data acquisition from strain gages, load transducers, pressure transducers, crack gages, etc. There are 40 channels to control the FASTER test fixture. The control channels include operation of the E/P valves, using a full proportional integral derivative (PID), closed-loop feedback error control process. A graphical interface program allows the operator to control the loads, speed, and type of test desired. Data acquisition from strain transducers, load transducers, pressure transducers, etc., are displayed on color monitors in real time and stored for off-line analysis.

## 2.4 Remote Controlled Crack Monitoring System

The Remote Controlled Crack Monitoring (RCCM) system, shown in Figure 7, was developed to track and record multiple crack formation and propagation during loading in real time. The RCCM system is a stand-alone, computer-based video data acquisition system capable of monitoring the entire fuselage panel test surface at several levels of magnification with a field of view ranging from 0.05" up to 14". The system consists of cameras mounted to two computer remote-controlled, high-precision translation stages and provides accurate and repeatable length measurements.

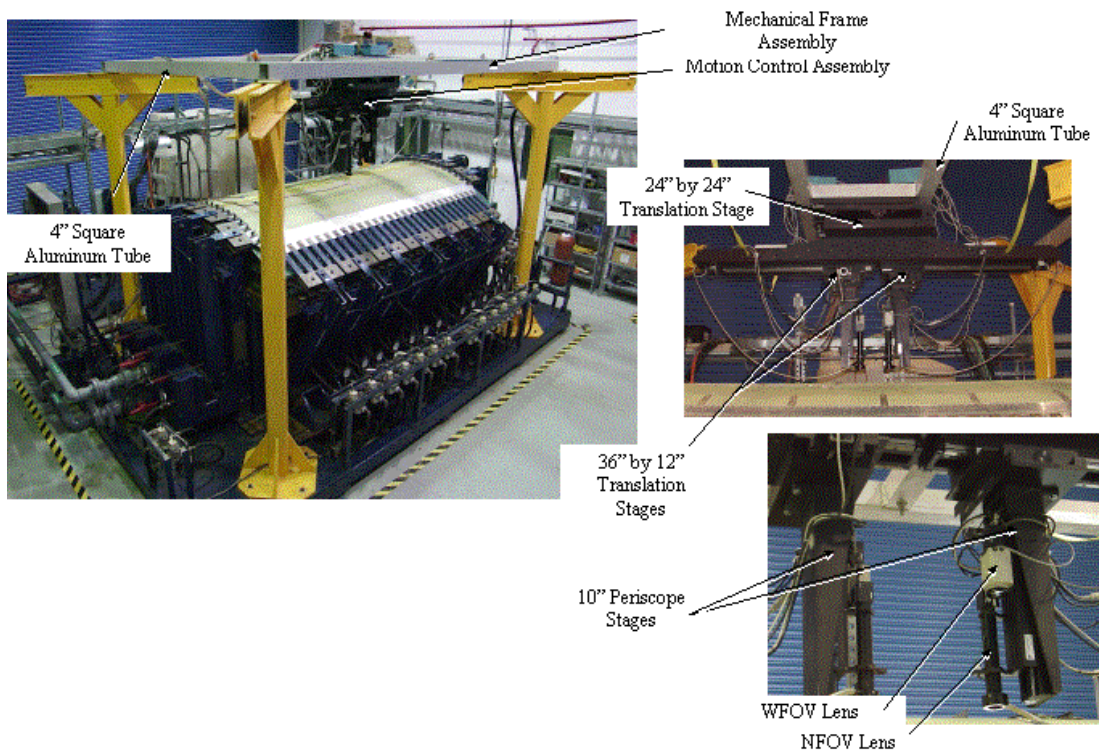


**Figure 7.** Photographs of FASTER facility and RCCM system

The RCCM system, comprises three main components: a mechanical frame assembly, a motion control assembly, and a video data acquisition system. The mechanical frame assembly is used to mount and place the motion control assembly over the test section of the panels while in the fixture. A large rectangular frame made from 4" square aluminum tubing is mounted on top of the four counterbalance columns of the fixture. A second section sits within the rectangular frame and can slide to provide longitudinal positioning of the motion control assembly. The third component fits within the second section for lateral positioning of the motion control assembly.

The motion control assembly is comprised of three bidirectional and two single-directional translation stages each having a 0.078" lead screw. A bidirectional translation stage provides 24" of overall travel in each direction. Two more bidirectional translation stages are mounted underneath the 24" bidirectional stage, each providing 36" of travel in longitudinal direction and 12" of travel in the lateral direction. Periscope stages are mounted to the two 36" by 12" bi-directional translation stages to provide translation in the z direction of 10".

The motion of the stages are remotely controlled by a computer via a joystick, mouse, and keyboard, which sends step and direction commands through a 50-pin ribbon cable to each of the eight motor driver modules. The stages are powered by 24-volt, 4-ampere, four-phase stepper motors that provide 200 full steps per revolution. The stepper motors driver modules further divide the step to ten increments providing motion resolution of 0.000039". The accuracy of the lead screws is 0.0039" per 10" of travel and bi-directional repeatability is 0.000236".

The video data acquisition assembly contains two black and white RS-170 format analog cameras operating at 30 frames per second with high-resolution 768 by 493 pixel chips. The two cameras are mounted to each of the two periscope stages. A high-magnification zoom lens (narrow-field-of-view (NFOV) lens) is attached to the first camera and provides a field-of-view ranging from 0.05" up to 0.5". The NFOV lens was modified to accommodate a simple belt-driven motor to control the zoom ring remotely. In addition, a fiber-optic ring light is attached to the end the NFOV lens to provide localized lighting that also can be controlled remotely. A zoom lens (wide-field-of-view (WFOV) lens) is attached to the second camera with a focal length range of 0.45" to 2.71" having complete motorized zoom, focus, and iris controls built-in. A +1 diopter and +2 diopter were added to the WFOV lens end to provide a field-of-view ranging from 2" up to 14".

Video data acquisition and reduction software provides real-time crack length measurement capabilities from the cameras on each stage. Using a cross-hair on the image as a reference, accurate measurements of crack length can be through the control of the translation stages. Up to 360 of the 768-by 493-pixel digital images can be captured continuously and stored in bitmap format at a rate of up to 30 frames per second. The software can playback the stored images. In addition, direct hook-up to monitors and video control recording (VCR) equipment is provided for continuous real-time monitoring and recording.

### 3 EXPERIMENTAL PROCEDURE

The matrix for several panels tested is highlighted in Table 1. For each panel listed in the table, the objective of the test, the panel description, the initial damage state, and the test type conducted are provided. In general, tests include strain survey under quasi-static loading conditions to ensure proper load introduction, fatigue loading to measure crack formation and growth, and residual strength test under quasi-static load conditions to measure the load carrying capacity.

**Table 1.** Test matrix

Specimen Designation	Test Objective	Panel Description	Initial Damage	Test Type
CVPA	Verify operational parameters of FASTER facility and establish experimental procedures.	Longitudinal splice panel removed from a retired narrow-body aircraft.	<ul style="list-style-type: none"> <li>As-Received</li> <li>Skin mid-bay skin crack</li> </ul>	<ul style="list-style-type: none"> <li>Strain survey</li> <li>Fatigue crack growth</li> </ul>
CVPB	Study fatigue crack initiation, growth, and distribution.	Longitudinal splice. Pristine panel manufactured per OEM specifications.	None	<ul style="list-style-type: none"> <li>Strain survey</li> <li>Fatigue crack growth</li> </ul>
CVP1	Determine effects of multiple cracks on fatigue crack growth and residual strength.	Longitudinal splice. Pristine panel manufactured per OEM specifications.	Lead crack in outer critical rivet row of joint. Severed central frame.	<ul style="list-style-type: none"> <li>Strain survey</li> <li>Fatigue crack growth</li> <li>Residual strength</li> </ul>
CVP2	Determine effects of multiple cracks on fatigue crack growth and residual strength.	Longitudinal splice. Pristine panel manufactured per OEM specifications.	Lead crack and small collinear multiple cracks in critical rivet row of joint. Severed central frame.	<ul style="list-style-type: none"> <li>Strain survey</li> <li>Fatigue crack growth</li> <li>Residual strength</li> </ul>
CVP3	Determine effects of multiple cracks on fatigue crack growth and residual strength.	Circumferential butt joint. Pristine panel manufactured per OEM specifications.	Lead crack in outer critical rivet row of joint. Severed central stringer.	<ul style="list-style-type: none"> <li>Strain survey</li> <li>Fatigue crack growth</li> <li>Residual strength</li> </ul>
CVP4	Determine effects of multiple cracks on fatigue crack growth and residual strength.	Circumferential butt joint. Pristine panel manufactured per OEM specifications.	Lead crack and small collinear multiple cracks in critical rivet row of joint. Severed central stringer.	<ul style="list-style-type: none"> <li>Strain survey</li> <li>Fatigue crack growth</li> <li>Residual strength</li> </ul>

#### 3.1 Panel Configurations

Typical panel dimensions are 120" in the longitudinal direction, 68" in the circumferential direction, with a radius of 66", as shown in Figure 8. The panels tested represent narrow-body fuselage structure with either a longitudinal lap splice or a circumferential butt joint. The panel size was selected so that the test section will contain large damage such as a two-bay crack with the central frame severed. The test section of the panel was sized in order to minimize the effect of the test fixture attachment points along the perimeter.

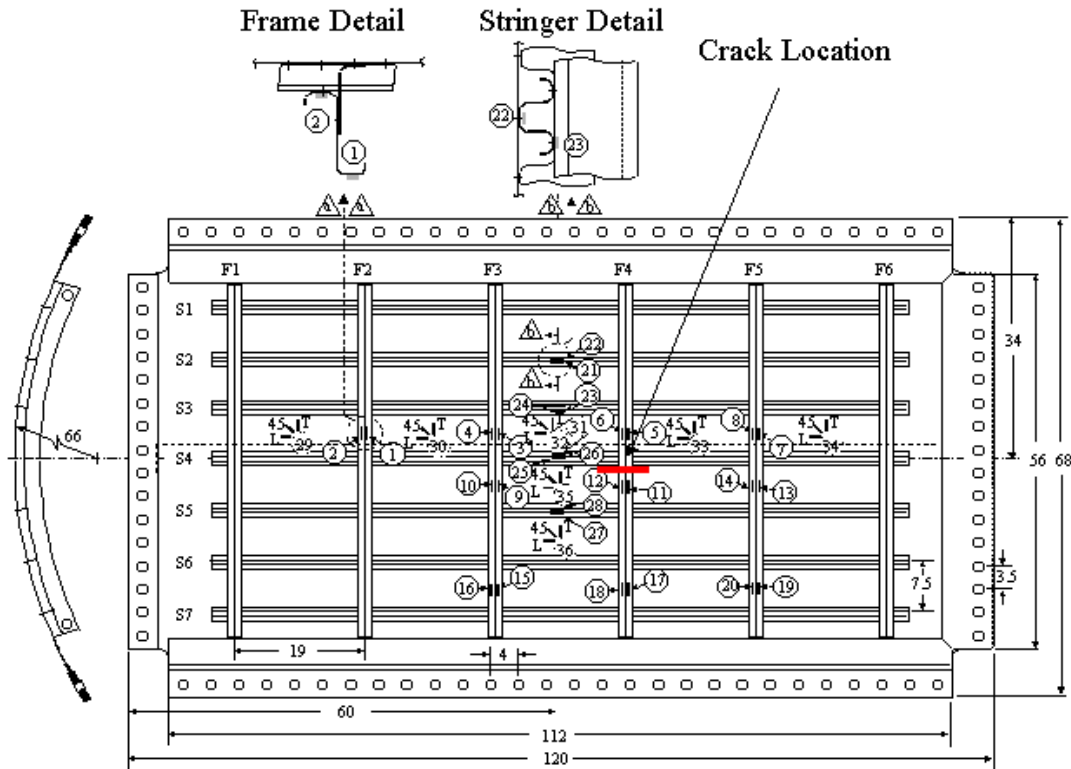


**Figure 8.** CVP1 and CVP2 panel configuration and strain gage locations

Each panel had six frames with a 19" spacing and seven stringers with a 7.5" spacing. The Z-shaped frames, L-shaped shear-clips, and hat-shaped stringers were 7075-T6 aluminum. Along the perimeter of the panel, reinforcing doublers with a length of 112" on the longitudinal sides and 56" on the hoop sides were added. Holes with a diameter of 0.5" were spaced approximately 4" apart on the longitudinal sides and 3.5" apart on the hoop sides to attach the whiffle tree assemblies which apply the load. There were 28 load application points on each longitudinal side and 16 load application points on each hoop side. Doublers were also added to the frame ends where they attach to the frame loaders. All panels were instrumented with 64 channels of strain gages.

Panel CVPA was the initial panel tested for verifying the FASTER facility operating parameters and establishing experimental test procedures for strain survey and fatigue crack growth as described in references 11 and 12. This panel was extracted from a retired narrow-body aircraft and contained a longitudinal lap splice. The skin was 2014-T6 aluminum with a thickness of 0.05". Initially, panel CVPA was tested in the as-received condition in a strain survey to ensure proper load introduction from the application points. A mid-bay crack was then inserted in the panels to establish crack bulging deflection and the fatigue crack growth measurement procedures.

Panel CVPB was tested to determine fatigue crack formation, growth, and distribution. This panel contained a longitudinal lap splice and represents a generic fuselage structure from a

narrow-body aircraft fabricated according to original equipment manufacturing (OEM) specifications. The panel was pristine with no initial damage. A strain survey was conducted to ensure proper load introduction and then subjected to constant amplitude fatigue loading. During fatigue loading, a rotating eddy-current probe was used to inspect for nonvisual cracks that develop under rivet heads in the lap joint area.

Panels CVP1 through CVP4 were tested to determine the effects of multiple cracks on the fatigue crack growth and residual strength of fuselage structure as outlined in reference 10. These panels also represent a generic fuselage structure from a narrow-body aircraft fabricated according to OEM specifications. Panel CVP1 contains a longitudinal lap splice with a lead crack. Panel CVP2 has the same configuration and lead crack as CVP1 with the addition of multiple, small cracks emanating from rivet holes ahead of the lead crack. Panel CVP3 has a circumferential butt joint with a lead crack. Panel CVP4 has the same configuration and lead crack as panel CVP3, with the addition of multiple, small cracks emanating from rivet holes ahead of the lead crack. These panels were subjected to a sequence of three tests: (1) strain survey under quasi-static loading; (2) fatigue test loading under constant amplitude loading; and (3) residual strength test under quasi-static loading up to fracture.

### 3.2 Test Conditions

The panels were subjected to the applied loadings listed in Table 2 for strain survey, fatigue crack growth, and residual strength tests. For the longitudinal lap joint panels, the applied load simulates the cylindrical pressurization that a section of the fuselage along the neutral axis would experience. For the circumferential butt joint panels, the applied load simulates a fuselage down-bending condition that a fuselage section along the crown of the aircraft would experience, where the longitudinal stress is 50% higher than the hoop stress.

**Table 2.** Applied Load Components

Panel	Maximum Load			
	Pressure (psi)	Hoop (lb/in)	Frame (lb/in)	Long. (lb/in)
CVPA	5.0	283.8	46.2	165.0
CVPB	16.0	878.6	177.4	528.0
CVP1	10.1	554.6	111.9	333.3
CVP2	10.1	554.6	111.9	333.3
CVP3	8.8	483.2	97.6	875.7
CVP4	8.8	483.2	97.6	875.7

For the strain survey tests, quasi-static loadings were applied in ten equal increments up to the maximum loads listed in Table 2 for the panels tested. For the fatigue crack growth tests, constant amplitude loading was applied at a frequency of 0.2 Hz with an R-ratio (minimum to maximum load) of 0.1 where the maximum loads are listed in Table 2. Crack growth of the lead crack and small multiple cracks was continuously monitored and recorded using the RCCM system. For the residual strength tests, the load was applied quasi-statically up to catastrophic failure proportional to the values listed in Table 2.

### 3.3 Verification Testing

To verify test results generated using the FASTER facility, comparisons were made with results from a full-scale test conducted on an aft fuselage section of a retired narrow-body aircraft. The aft fuselage section was mounted on a strong back fixture and pressurized quasi-statically from 0 to 7.8 psi for three tests. Strains in a section of the test article, which closely resembled the panels tested, were compared with strains measured at similar locations in the longitudinal lap joint panel, CVPB.

## 4 ANALYSIS

Geometric nonlinear finite element analyses were conducted to support the tests using the commercial finite element code ABAQUS 5.8 [13]. Two analyses were conducted for each panel: the first to predict the strain distributions and the second to compute the mixed mode stress-intensity factor (SIF) solutions using the Modified Crack Closure Integral (MCCI) method [14, 15]. A full description of the analysis conducted is provided in references 10, 11, and 12. In general, panels were modeled using two-dimensional shell elements with each node having six degrees of freedom. Figure 9 shows the global view of a typical finite element model of panel CVP3. Four-noded shell elements were used throughout to model the skin, frames, shear clip, stringers, and intercostals except near the crack tips. In the immediate vicinity of the crack tips,

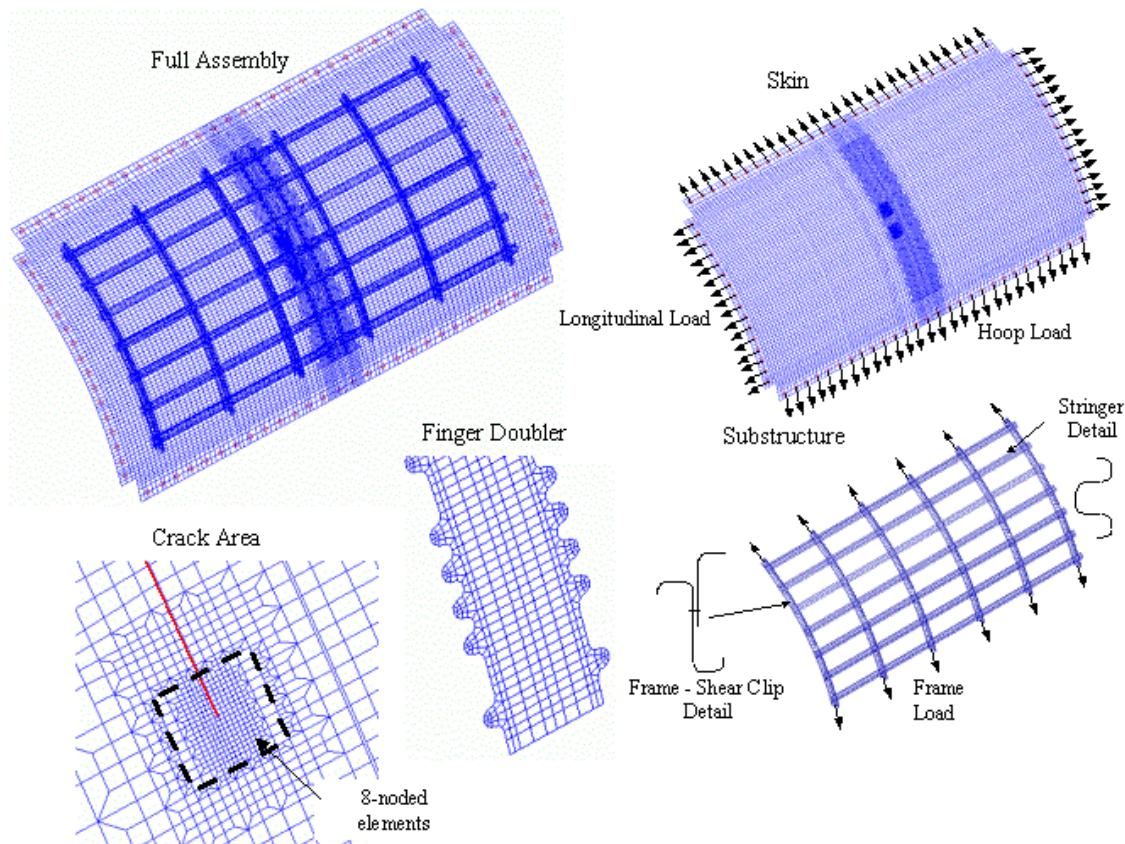


**Figure 9.** Finite element model of CVP3 showing full assembly and substructure components

eight-noded shell elements were used. The models contained the major geometric details of the panels including the cross-section properties and dimensions of the substructure (frames, stringers shear-clip, intercostals), the finger doublers, and the load attachment doublers. Beam elements were used to model the rivets that connected the substructures with the skin and the substructures to one another. Typically, the panel models had 250,000 degrees of freedom. The load conditions specified in Table 2 were simulated in the analysis. For the hoop, frame, and longitudinal loads, nodal point forces were applied at the load application points in the actual test as shown by the arrows in Figure 9. Internal pressure was applied to the inner surface of the skin.

## 5 RESULTS AND DISCUSSION

Representative results generated using the FASTER facility are outlined in the subsequent sections from of the strain and deformation survey, fatigue crack growth testing, and residual strength testing.

### 5.1 Strain and Deformation Survey

The strain distribution was measured and predicted under quasi-static load conditions using the load components listed in Table 2 for the panels tested. Representative results from panel CVPB are shown in Figure 10. The hoop strain in the skin at a mid-bay location is shown in the figure as a function of applied pressure. The load was applied in ten equal increments up to the

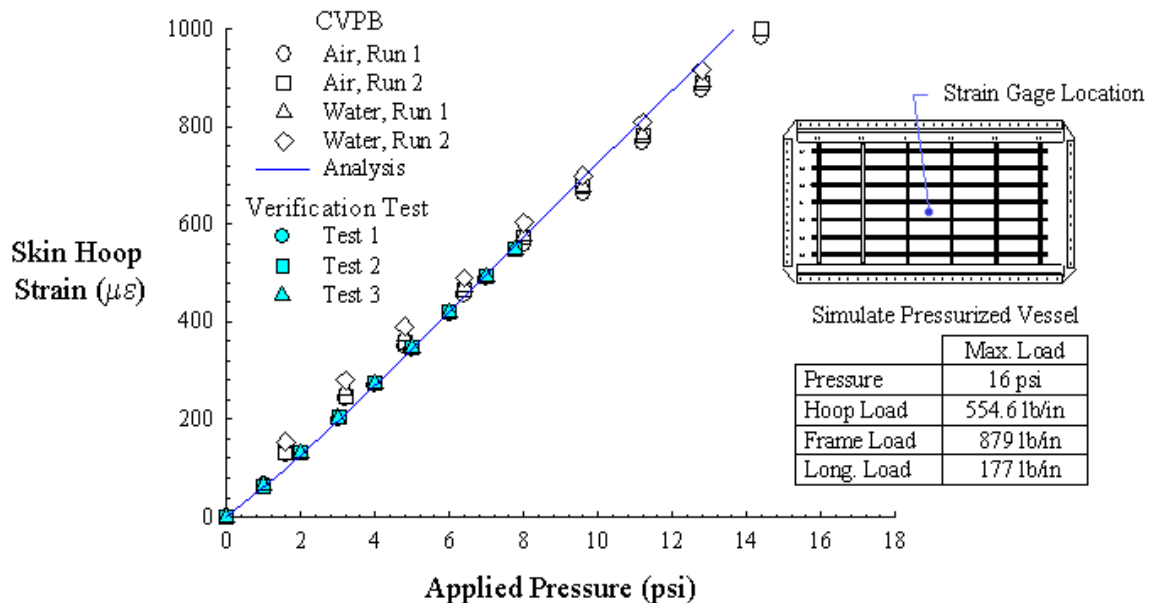


**Figure 10.** Hoop strain at skin mid-bay in panel CVPB and verification full-scale test article maximum values listed Table 2, which simulates a cylindrical pressurization. The test was repeated twice using water and twice using air. As shown in the figure, the strains are nearly identical for all four runs. As expected, there were no differences in the results when air or water was used to pressurize the panel.

The results from the full-scale verification test measured in the skin mid-bay location are also plotted in Figure 10. As shown in the figure, the results from panel CVPB agree well with the full-scale verification test results for the given load levels. This indicates that the applied loading to panel CVPB correctly simulates the pressurization of a fuselage structure. Also shown in Figure 10 is the prediction using ABAQUS as described previously. The prediction, shown by the solid line, is in good agreement with the experimental data validating the finite element analysis.

The hoop strain in the skin for panels CVP1 and CVP2 (contained multiple cracks) is shown in Figure 11. The values shown for each panel are the averages of the four tests conducted. As shown in the figure, the magnitudes of the measured strains in both panels were similar and the distributions were nearly uniform in the middle of the panels. Thus, multiple cracking did not effect the overall strain response.

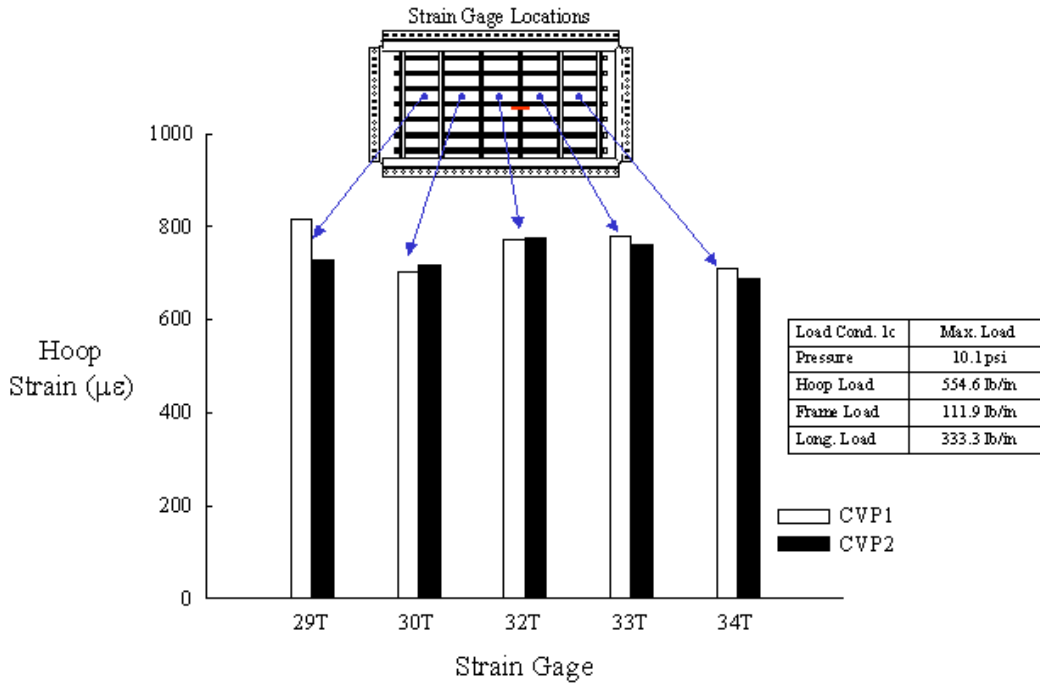


**Figure 11.** Hoop strain distribution in the skin mid-bay in panels CVP1 and CVP2

In general, similar trends in strain gage data were obtained at the other gage locations in the panels tested. That is, experimental results were very repeatable and the analytical predictions were in good agreement with the test results. Measured strains were nearly uniform in the middle of the panel. This provides confidence that the applied loads were introduced properly, and the models have enough fidelity to capture the mechanical response. In addition, the small multiple cracks had no effect the global strain response.

The measured and predicted out-of-plane displacements along the length of the crack at a distance of 0.15" from the crack are shown in Figure 12 for panel CVPA. The half crack length was  $a_f = 3.33$ " for the displacements shown. As expected, the out-of-plane displacement is highest at the centerline and the shape of the crack bulging profile is symmetric about the

centerline. Results from analyses shown by the solid curve were in excellent agreement with the experimental data.

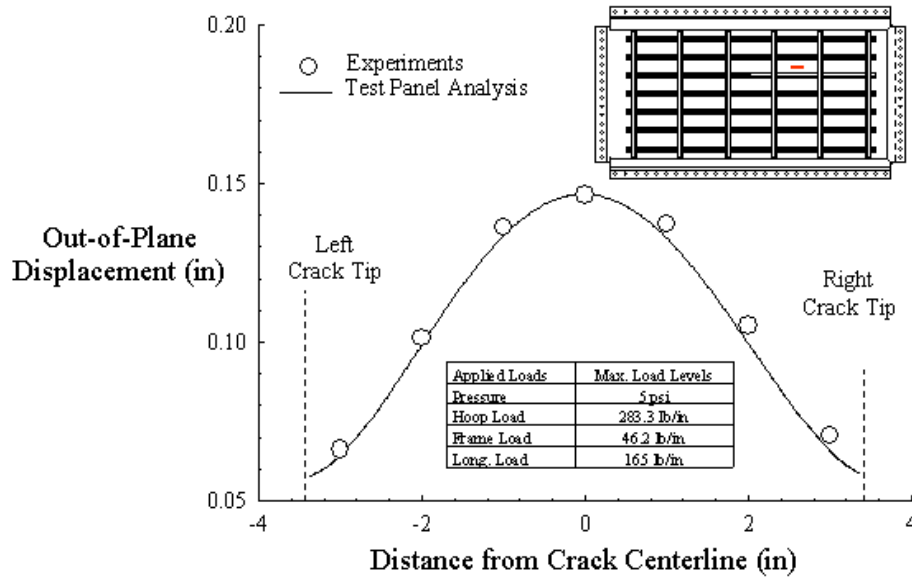


**Figure 12.** Crack bulging profile in panel CVPA

## 5.2 Fatigue Crack Growth

The fatigue crack growth was measured in all panels under constant amplitude loading using the maximum values listed in Table 2. The growth of the lead crack and the multiple cracks was recorded and monitored. Representative results are presented here in. Images of crack extension under fatigue loading from the RCCM system are shown in Figure 13 for panel CVP1.

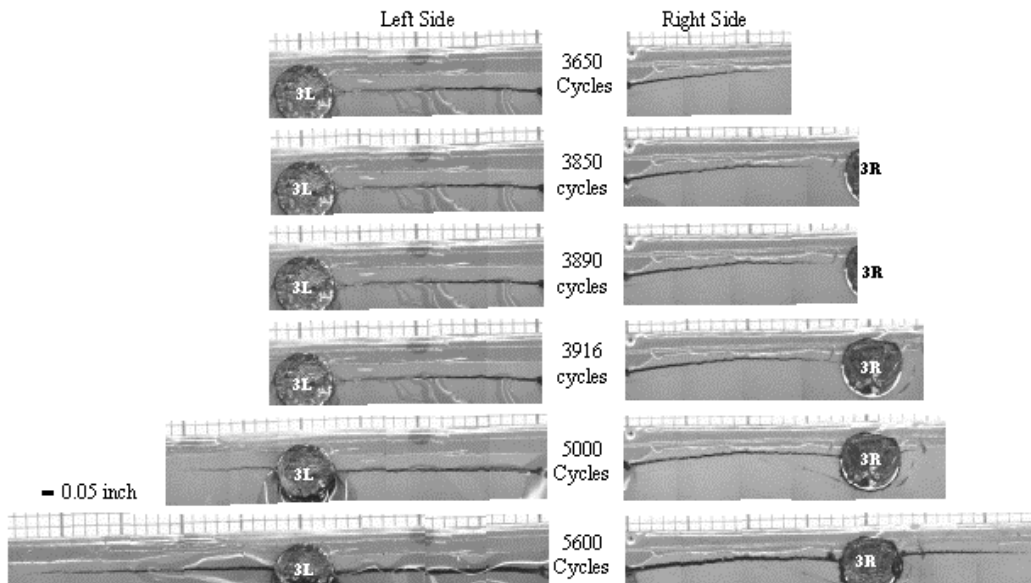


**Figure 13.** Images of crack growth in panel CVP1 during fatigue loading using RCCM system

The images illustrate the progression of damage from the original slit to the first adjacent rivet (3R and 3L). The block size of the grid paper on the top of each image is 0.05". In general, the crack extension was symmetric and collinear indicating a symmetric load in the region of the crack tips.

The fatigue crack growth behavior of panels CVP3 and CVP4 (contained multiple cracks) is shown in Figure 14. The initial damage consisted of a two-bay lead crack approximately 7" in length with the central stinger saw cut. The applied load simulates a fuselage down-bend condition where the longitudinal stress was 50% higher than the hoop stress. In the figure, the circular and square symbols represent the measured crack lengths of the left and the right crack

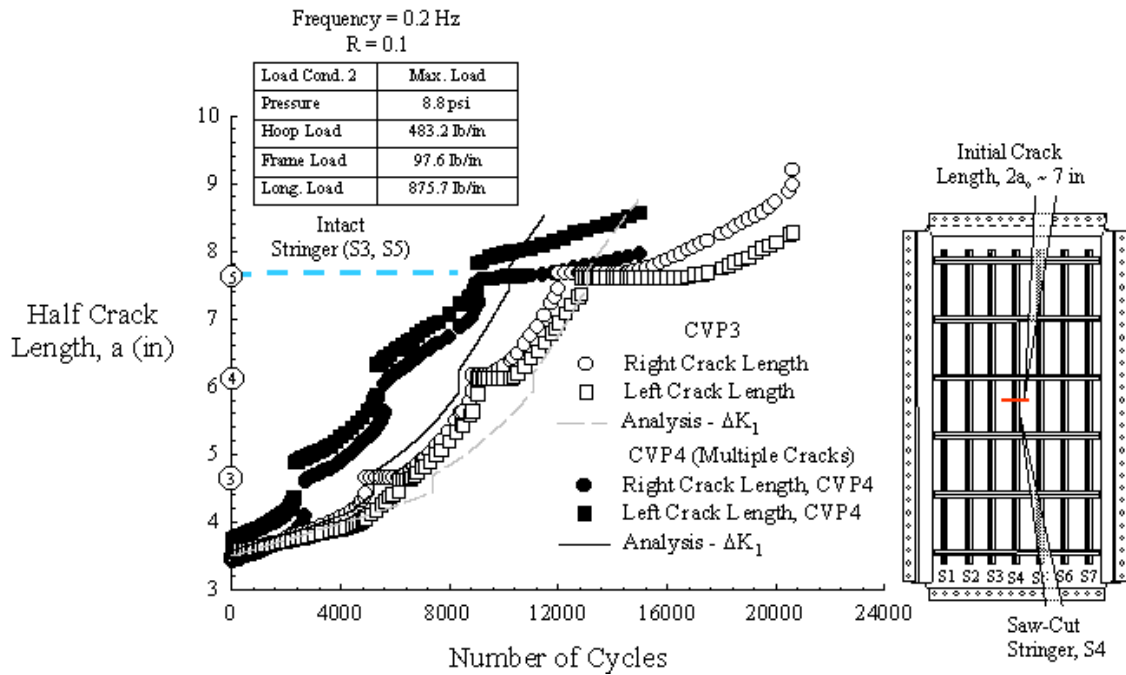


**Figure 14.** Half crack length during fatigue loading for panels CVP3 and CVP4

tips, respectively, from both panels. The numbers inside the circles along the y axis indicates the locations of the rivets. For panel CVP3, crack growth across a rivet hole is indicated by a vertical jump in the data, where the crack length instantaneously increases by a length equal to the hole diameter. The horizontal segments shown in the plot indicate the incubation period or the number of cycles for the crack to reform on the opposite side of the rivet hole. For panel CVP4, which contained multiple cracks, the vertical jumps in the experimental data indicate the point when the lead crack and small multiple crack linked up. When this happened, the crack length increased instantaneously by the diameter of the rivet hole plus the lengths of the small cracks at that rivet. There was no crack reformation required. The small crack at the rivet hole on the opposite side became the new lead crack front. As a result, the number of cycles to grow the lead crack to the third rivet hole in panel CVP4 was approximately 27% less than that in panel CVP3. At the third rivet hole on either side, 5R and 5L, the crack had just reached the first intact stringers (S3 and S5). The additional stiffness added by the stringers increased the

incubation period for panel CVP3 and decreased the subsequent crack growth rate for both panels.

The Mode I SIF range was used in a cycle-by-cycle crack growth analysis program to predict the fatigue crack growth in panels CVP3 and CVP4, also shown in Figure 14. The analysis based on the Mode I SIF range was in good agreement with the test data for crack growth in both panels until the crack reached the intact stringer. Little crack bulging was observed during the test, indicating that the crack growth was primarily due to Mode I loading.

### 5.3 Residual Strength

The residual strength of the panels was measured under quasi-static loading conditions. An example from the residual strength test of panels CVP1 and CVP2 (contained multiple cracks) is shown in Figure 15 where the square and circular symbols represent the crack extension for the

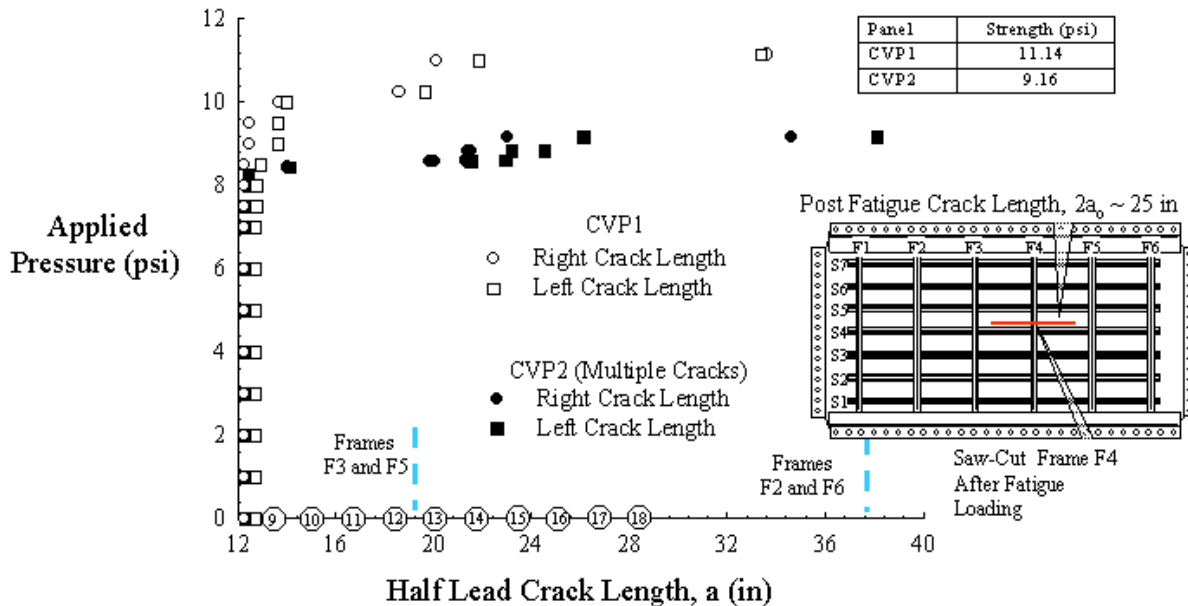


**Figure 15.** Crack extension during residual strength tests for panels CVP1 and CVP2

left and right crack tips, respectively. The initial damage consisted of a two-bay lead crack approximately 25" in length with the central frame saw cut. The numbers inside the circles along the x axis indicate a rivet location. During the test, cylindrical pressurization was applied quasi-statically, and the crack extension measured up to panel failure. The initial stages of loading, slow stable crack extension was observed in both panels up to 10.25 psi pressure for panel CVP1 and 8.5 psi pressure for panel CVP2. Then, the crack grew rapidly through rivets 9 through 11 on both the right and left side to the first intact frames (F3 and F5) for both panels and then were arrested. An increase of pressure was required to grow the cracks past the frames in both panels and stable crack extension continued until catastrophic failure occurred at 11.14 psi for panel CVP1 and 9.16 psi for panel CVP2. The presence of multiple cracks reduced the residual strength by approximately 20%.

## 6 CONCLUDING REMARKS

The Full-Scale Aircraft Structural Test and Evaluation Research (FASTER) facility located and operated at the FAA William J. Hughes Technical Center was established to assess the structural integrity of aircraft fuselage structure. The FASTER test fixture is capable of applying realistic flight load conditions to large sections of a fuselage structure. Both quasi-static and long-term durability spectrum loadings can be applied including differential pressure, longitudinal, hoop and shear load in the skin, and hoop load in the frames. The system was designed using commercial-off-the-shelf (COTS) components and to operate in an environment requiring minimal infrastructure support. Safety was considered in the design of the system by using water as the loading media. Simple loading mechanism consisting of levers, fulcrums, and water actuators are used to economically introduce complex mechanical loading. This simplified mechanical design concept, in conjunction with a computer control and data acquisition system, presents a test system that is user friendly, has low-cost maintenance, is inherently safe, and is highly versatile.

Representative test and analyses results obtained for typical narrow-body fuselage structure consisting of skin, frames, shear clips, stringers, and either longitudinal splice or circumferential joints were presented. Strain survey tests were conducted under quasi-static loading conditions on test panels to verify proper load transfer from the load application points to the panels. Comparison with an independent full-scale test conducted on an aft fuselage section of an actual aircraft with similar structural details to the panels tested and comparisons with detailed finite element analysis results confirmed appropriate applied load conditions. Crack growth under fatigue loading conditions was measured and recorded using the Remote Control Crack Monitoring (RCCM) system up to a predetermined crack length. Finally crack extension and residual strength were measured under quasi-static loading conditions.

## 7 REFERENCES

1. Newman, J. C., Jr., "A Crack-Closure Model for Predicting Fatigue Crack Growth Under Aircraft Spectrum Loading," American Society for Testing and Materials, USA, Special Technical Publication 748, 1981, pp. 53-84.
2. Newman, J. C., "Finite Element Analysis of Crack Growth Under Monotonic and Cyclic Loading," American Society for Testing and Materials, USA, Special Technical Publication 637, 1977, pp. 56-80.
3. Harris, C. E., Newman, J. C., Piascik, R. S., and Starnes, J. H., "Analytical Methodology for Predicting the Onset of Widespread Fatigue Damage in Fuselage Structure," *Proceedings of FAA-NASA Symposium on Continued Airworthiness of Aircraft Structures*, DOT/FAA/AR-97/2, July 1997.
4. Atluri, S. N. and Nishioka, T., *Engineering Fracture Mechanics*, Vol. 20, 1984, pp. 209-244.

5. Wang, L., Brust, F. W., and Atluri, S. N., "Predictions of Stable Growth of a Lead Crack and Multiple-Site Damage Using Elastic-Plastic Finite Element Alternating Method (EPFEAM)," *Proceedings of FAA-NASA Symposium on Continued Airworthiness of Aircraft Structures*, DOT/FAA/AR-97/2, July 1997.
6. Broek, D., "Effects of Multi-Site Damage on the Arrest Capability of Aircraft Fuselage Structures," *FractuREsearch*, Inc., USA, TR 9302, 1993.
7. Swift, T., "Widespread Fatigue Damage Monitoring—Issues and Concerns," *Proceedings of 5<sup>th</sup> International Conference on Structural Airworthiness of New and Aging Aircraft*, Federal Republic of Germany, DGLR-Bericht 93-02, 1993, pp. 133-150.
8. Bakuckas, J. G., Nguyen, P. V., and Bigelow, C. A., "Bulging Factors for Predicting Residual Strength of Fuselage Panels," *Proceedings of the 19th Symposium of the International Committee on Aeronautical Fatigue*, ICAF 97, Edinburgh, United Kingdom, 1997, pp. 179-196.
9. Tan, P.W., Bigelow, C. A., and Bakuckas, J. G., Jr., "An Integrated Methodology for Assessing Widespread Fatigue Damage in Commercial Aircraft," *Seventh International Fatigue Conference Fatigue '99*, Beijing, Peoples Republic of China, June 8-12, 1999.
10. Bakuckas, J. G. Jr., "Full-Scale Testing of Fuselage Structure Containing Multiple Cracks," DOT/FAA/AR-01/46, 2001.
11. Bakuckas, J. G., Jr., Bigelow, C. A., and Tan, P. W., "The FAA Full-Scale Aircraft Structural Test Evaluation and Research (FASTER) Facility," *Proceedings from the International Workshop on Technical Elements for Aviation Safety*, Tokyo, Japan, pp. 158-170, 1999.
12. Bakuckas, J. G., Jr., Akpan, E., Zhang, P., Bigelow, C. A., Tan, P. W., Awerbuch, J., Lau, A., and Tan, T. M., "Experimental and Analytical Assessments of Multiple-Site Cracking in Aircraft Fuselage Structure," *Proceedings of the 20th Symposium of the International Committee on Aeronautical Fatigue*, Seattle, Washington, USA, July 14-15, 1999.
13. ABAQUS Version 5.8, Hibbitt, Karlsson, and Sorensen (HKS), 1080 Main Street, Pawtucket, RI 02860, USA, 1998.
14. Rybicki, E. F. and Kanninen, M. F., "A Finite Element Calculation of Stress-Intensity Factors by a Modified Crack Closure Integral," *Engineering Fracture Mechanics*, Vol. 9, pp. 931-938, 1977.
15. Viz, M. J., Potyondy, D. O., and Zehnder, A. T., "Computation of Membrane and Bending Stress-Intensity factors for Thin, Cracked Plates," *International Journal of Fracture*, Vol. 72, pp. 21-38, 1995.